

1 **Lead and slant on the geometry of coiling in gastropods**

2

3 Ido Filin ¹ *

4 ¹ No author affiliation.

5 * Corresponding author. E-mail: ido@filin.fi

6

7 Running headline: Geometry of coiling.

8 Supplementary material: SI appendix.

9 The author(s) declare(s) no conflict of interest.

10 This manuscript was compiled on 30 April 2026.

11 **Abstract**

12 Molluscan shells have been studied with various geometric models. Here I show that
13 *lead angle*, the defining slope of a conical helix, emerges as a more useful parameter in
14 morphometric analyses and (adaptationist) interpretation of covariation in coiling
15 parameters. The widely used apical semiangle becomes redundant and uninformative, a
16 passive consequence of taxon-specific lead angles and plasticity in growth (expansion rate).
17 Treating coiled shells as conical helices, and extending to *logarithmic slant helices* (curves of
18 precession), provides insights into ontogenetic allometry, irregular coiling, past models, and
19 unifying fixed- and moving-frame approaches.

20

21 **Keywords:** allometry, conchology, logarithmic spiral, ontogeny, slant helix, theoreti-
22 cal morphology,

23 **Note**

24 The equiangular, or logarithmic, spiral has a long and distinguished history, going back to
25 Descartes, Torricelli, Christopher Wren, Newton, Halley, and the Bernoullis (Thompson
26 [1942] 1992; Archibald 1918; Hammer 2016). Its application in biology, however, only picked
27 up with Canon (Henry) Moseley and Carl Friedrich Naumann around 1840, who applied it to
28 the study of molluscan shells, coinciding with the rapid development of paleontology in the
29 19th century (Moseley 1838, 1842; Naumann 1845; Thompson [1942] 1992; Raup 1966;
30 Vinarski 2014). Much of this earlier work on modeling and measurement of shells is
31 thoroughly and eloquently summarized in D’Arcy Thompson’s *magnum opus* “On Growth
32 and Form” (Thompson [1942] 1992).

33 In “The geometry of coiling in gastropods”, Raup (1961) sketched an earlier version of his
34 parameter set for coiled geometries, that would later develop into theoretical morphology
35 and the morphospace concept (Raup & Michelson 1965; Raup 1966, 1967; McGhee 1999;
36 Gerber 2017). Essentially, though, Raup’s model is a reformulation of the original *conispiral*
37 parametrization of Moseley (1838) and Thompson ([1942] 1992) – a logarithmic spiral
38 wrapped around a cone of *apical semiangle*, β , rather than winding on a plane (planispiral
39 coiling, $\beta \rightarrow \pi/2$; Fig. 1A,D). Its defining feature is a fixed *spiral angle*, α , between the tangent
40 of the spiral and its pole (or apex of the cone; hence, equiangular; Fig. 1A).

41 Conical logspirals also arise from fixed standardized *curvature* and *torsion* in the
42 *differential geometric* formulation of Okamoto (1988), a local (moving) frame analysis
43 (Fig. 1B) that he named the ‘growing tube’ model. A third alternative parameterization views
44 the conical logspiral as a *conical helix* (Fig. 1C). The defining feature of a helix (more
45 accurately, general or generalized helix, or curve of constant slope; Nutbourne & Martin
46 1988; Scofield 1995; Rice 1998; SI) is the constant angle its tangent makes with some fixed
47 direction. This direction determines the coiling axis, and the constant slope will be measured
48 in this study by the downward angle of the coil, or helical thread, termed *lead angle*, λ in
49 Fig. 1D. (Preserving here the distinction between ‘pitch’ and ‘lead’, in the case of

50 multi-thread or -strand helical structures, i.e., double or triple helices, or multi-start screws;
51 see SI for more on terminology). If the coils wrap around a cone ($0 < \beta < \pi/2$), rather than a
52 cylinder ($\beta \rightarrow 0$; the familiar circular helices of springs and corkscrews), such a conical helix
53 is also a logarithmic conispiral. I dub this third parameterization *conihelical*.

54 In the words of D’Arcy Thompson, “It seems a complicated affair; but it is only a pathway
55 winding at a steady slope up a conical hill ... a certain ensemble, or bunch, of these spiral
56 curves in space constitutes the self-similar surface of the shell” (Thompson [1942] 1992). In
57 this note, I explore how conical helices and their “steady slope”, or lead angle, have
58 underappreciated implications to morphometrics, interpretations of covariation in coiling
59 parameters, and unifying *fixed-* and *moving-frame* approaches to theoretical morphology. In
60 addition, conical helices can be extended to *slant helices*, particularly the *logarithmic slant*
61 *helix* that I present here, to gain better understanding of ontogenetic allometry, irregular
62 coiling, and previously formulated models of allometric spirals.

63 As hinted in the above quote, a shell is not a single conispiral, but a three-dimensional
64 structure made of “a bunch” of such spirals — the *multispiral* approach (Fig. 1E; also called
65 multivector; Thompson [1942] 1992; Bayer 1978; McGhee 1978, 1999; Savazzi 1990).
66 Alternatively, a shell can be described by a *generating curve*, a closed figure that sweeps
67 through space along a spiral *centerline* (Fig. 1F; Thompson [1942] 1992; Raup 1961, 1966;
68 Okamoto 1988; roughly corresponding to the ‘aperture trajectory’ of Stone 1995,
69 ‘curve-skeleton’ of Monnet *et al.* 2009, ‘ontogeny axis’ of Liew & Schilthuizen 2016, or
70 ‘internal spiral’ of Larsson *et al.* 2020). While called fictitious and an artificial construction
71 (Moulton *et al.* 2012; Moulton & Goriely 2012), the centerline seems a necessary evil, being a
72 central feature of most theoretical morphological and morphometric shell models (Raup
73 1966; Okamoto 1988; Liew & Schilthuizen 2016; Larsson *et al.* 2020; eventually, also Moulton
74 & Goriely 2012 use it).

75 In self-similar isometrically growing conihelical shells, the different spirals that make the
76 shell’s surface, by geometric necessity, differ in spiral angle, α , apical semiangle, β , and lead
77 angle, λ (Fig. 1E). However, they all share a single common value of exponential *expansion*

78 rate, γ , with respect to revolution angle, θ (Illert 1983). Given linear measures of shell size,
 79 such as aperture size, a and b (Fig. 1F), centerline radius and height, r and z (Fig. 1D), or
 80 centerline *arclength*, s , measured from the pole (or conical apex), one can define separate
 81 expansion parameters for each. However, for self-similar conihelical shells, these expansion
 82 rates are all equal, $\gamma_s = \gamma_a = \gamma_b = \gamma_z = \gamma_r = \gamma$. Alternatively, growth and size can be measured
 83 w.r.t arclength, s , rather than revolution angle, θ . For example, the relations $a(s)$ and $b(s)$, for
 84 aperture size, introduce Ackerly's (1989a) *dilation* parameter, which I denote here by
 85 $q_a = da/ds$ and $q_b = db/ds$. In isometric conihelical shells, q_a and q_b are constants,
 86 representing the opening angles of the expanding 'trumpet' or 'cone' (Ekaratne & Crisp 1983;
 87 Ackerly 1989a; Vermeij 2002) that is coiled upon itself to make the spiral shell. Dilation
 88 factors for centerline r and z are just $q_r = \cos \alpha \sin \beta$ and $q_z = \sin \lambda = \cos \alpha \cos \beta$.

89 A set of formulas relates the conispiral, conihelical, and differential geometric
 90 parameterizations to each other and to expansion rates. One such formula is the
 91 aforementioned expression for q_z , relating lead angle, λ , to spiral angle, α . For expansion
 92 rate,

$$93 \quad \cot \alpha \sin \beta = \gamma \quad (1)$$

94 (Moseley 1842; Thompson [1942] 1992; Raup & Graus 1972; Løvtrup & von Sydow 1974;
 95 Ekaratne & Crisp 1983; Illert 1983). Gastropod shells usually exhibit several complete whorls.
 96 Consequently, expansion rate is typically small, $\gamma \leq 0.2$ (Thompson [1942] 1992; Cameron
 97 1981), leading to a similar, approximate, expression for the conihelical parameterization,

$$98 \quad \tan \lambda \tan \beta \approx \gamma \quad (2)$$

99 (the exact expression being $\tan \lambda \tan \beta = \gamma / \sqrt{1 + \gamma^2}$; see SI for discussion of approximation
 100 errors), demonstrating the three-way covariation of expansion rate, apical semiangle and
 101 lead angle.

102 Many empirical studies of shell coiling, in the past 50 years, have provided estimates of
 103 Raup's T and W parameters; or in terms of this study, $\tan \beta = 1/T$ and $\gamma = \ln W/2\pi$
 104 respectively. Covariation of $\tan \beta$ and γ may point to adaptation, such as for mechanical

105 strength, postural stability or economical shell construction (Raup 1966; Noshita *et al.* 2012;
106 Okabe & Yoshimura 2017; Páll-Gergely *et al.* 2024), and is usually interpreted through Raup's
107 (1966) condition for tight coiling, or whorl overlap, $\tan \beta > \sinh(\pi\gamma)$, given circular apertures
108 (SI). (Alternatively, $\sin \beta > \tanh(\pi\gamma)$); corresponding to the expression by Clarke *et al.* 1999,
109 accounting for the typo in their equation, and the difference in definition of apical angle; SI).
110 However, for small γ , typical of most gastropods, the whorl overlap boundary is practically
111 indistinguishable from the seemingly arbitrary condition $\lambda < \arctan(1/\pi)$ (0.318 or 17.66°;
112 Fig. 2A; SI). Similar conditions can be formulated for non-circular apertures (SI). A geometric
113 constraint on lead (or spiral) angle, combined with variation in growth rate (shell expansion),
114 can therefore produce, given Eq.[2], the empirically observed direct relation between $\tan \beta$
115 and γ .

116 Past hints to the relative constancy of lead angles can also be glimpsed from observations
117 of ontogenetic patterns, where measurements of $\tan \beta$ and γ at different whorls, or
118 developmental stages, vary together so to preserve an almost fixed ratio (e.g., Newkirk &
119 Doyle 1975; Hutchinson 1989; Clarke *et al.* 1999). In particular, Ekaratne & Crisp's (1983)
120 shell-height-to-arclength-ratio contains a $1/\sec \alpha \sec \beta$ factor, which is just $q_z = \sin \lambda$ of this
121 study. In fact, their formula can be rewritten as $H/s = z/s + b/s = q_z + q_b = \sin \lambda + q_b$ (SI).
122 Lead angle, therefore, a defining feature of conical helices, emerges as a more useful
123 parameter for interpreting morphometric (co)variation (Fig. 2B). Variation in apical
124 semiangle (β ; Fig. 2A) follows as a passive consequence of growth (variation in γ) and
125 geometry (lead angle, λ) of the expanding centerline spiral (Eq.[2]).

126 Lead angle, however, is expected to vary ontogenetically to some degree. For example,
127 Savazzi (1990) discussed deviated protoconchs (see also Frýda & Ferrová 2011); van Osselaer
128 & Grosjean (2000) fitted conispirals piecewise to several species, and showed three
129 ontogenetic phases – protoconch, and early and late conispiral phases – with different
130 coiling parameters; and Newkirk & Doyle (1975) reported values of coiling parameters for
131 embryos and adults in a study of geographic variation in the rough periwinkle, *Littorina*
132 *saxatilis* (Fig. 2).

133 Variation in lead angle can be further understood by considering the differential geometric
134 parameterization. In helices, coiling angle per unit of centerline arclength, $d\theta/ds$, is
135 measured by the norm of the *Darboux vector*, $\mathbf{u} = u\hat{\mathbf{u}}$, the rotation vector of the Frenet frame
136 along its defining space curve (Fig. 1B; Chouaieb *et al.* 2006; Goriely 2017). In generalized
137 helices, $\hat{\mathbf{u}}$ coincides with the fixed coiling axis. The norm of the Darboux vector, $\|\mathbf{u}\| = u$, is
138 the ‘compound curvature’ of Nutbourne & Martin (1988), the ‘first alternative curvature’ of
139 Güzelkardeşler & Şahiner (2024), and the familiar $\sqrt{\kappa^2 + \tau^2}$ of differential geometric literature
140 (also D_G and A_G of Noshita 2014 and Noshita *et al.* 2016, who used Okamoto’s growing tube
141 formulation; clearly related in their expressions to angular rate, $d\theta/ds$). In this note, I refer
142 to u as *local coiling*. The constant lead angle of general helices is determined by the
143 torsion-curvature ratio, $\tan \lambda = \tau/\kappa$, $\kappa = u \cos \lambda$, and $\tau = u \sin \lambda$.

144 Conical helices are further defined by local coiling that is inversely proportional to
145 arclength, s (Nutbourne & Martin 1988). We can, therefore, write $u = \tilde{u}/s$, where \tilde{u} is
146 constant dimensionless *standardized local coiling* (though the ‘standardization’ here is
147 different than Okamoto’s). Arclength expansion rate, γ_s , is then related to (standardized)
148 local coiling by the simple and intuitive relation $\gamma_s = 1/\tilde{u}$ (SI). As local coiling and curvature
149 increase, the conical helix coils tighter, and less arclength growth and radial expansion is
150 gained per full revolution. Hence, more whorls are required for a specified amount of
151 (relative) growth. This helps to explain the association of high-spired species with large
152 numbers of whorls (Cain 1980) and Gould’s so-called “jigsaw constraint”, originally observed
153 in his study of *Cerion* (Gould 1989; Béguinot 2021).

154 Allometric modifications of conical helices, such as the logarithmic *helicospiral* model,
155 derived many times in various guises (essentially, $\gamma_z \neq \gamma_r$; Kohn & Riggs 1975; Bayer 1978;
156 Cortie 1989; Schindel 1990; Savazzi 1990; Fowler *et al.* 1992; Stone 1995; Tursch 1997; van
157 Osselaer & Grosjean 2000; Urdy *et al.* 2010; Swan 2015; Larsson *et al.* 2020), and Harary &
158 Tal’s (2011)’s ‘natural 3D spiral’, do not have constant lead angles, and therefore, are not
159 generalized helices. Rate of change in lead angle, $\lambda' = d\lambda/ds$, is equivalent to the ‘second
160 alternative curvature’ of Uzunoğlu *et al.* (2016) and Güzelkardeşler & Şahiner (2024) (see SI).

161 If $\lambda' \neq 0$, the Darboux vector of local coiling and the fixed coiling axis of the helicospiral do
 162 not coincide, as the former now precesses around the latter (Fig. 1G). The precession axis is

$$163 \quad \mathbf{w} = w\hat{\mathbf{w}} = \mathbf{u} + \lambda'\hat{\mathbf{n}} = u\hat{\mathbf{u}} + \lambda'\hat{\mathbf{n}}, \quad (3)$$

$$w = \|\mathbf{w}\| = \sqrt{u^2 + (\lambda')^2} = \sqrt{\kappa^2 + \tau^2 + (\lambda')^2},$$

164 dubbed here respectively vector and rate of *global coiling*. This total coiling rate contains
 165 both a local coiling component, u , and a λ' component (first and second ‘alternative
 166 curvatures’ of [Uzunoğlu et al. 2016](#) and [Güzelkardeşler & Şahiner 2024](#); generalized helices
 167 are obtained when $\lambda' = 0$).

168 Four decades ago, [Løvtrup & Løvtrup \(1988\)](#) attempted to “move the β parameter down to
 169 the mantle edge”. In other words, derive a parameter of global shell shape from local
 170 processes occurring at the aperture. [Løvtrup & Løvtrup](#)’s partial solution was to replace β
 171 with the ratio of maximum and minimum growth rates around the aperture. An explanation
 172 that [Hutchinson \(1990\)](#) debunked shortly after. Through Eqs.[1] and [2], however, the apical
 173 semiangle can indeed be “eliminated”, or “moved down” to the aperture, as γ , α , and λ are
 174 defined at the growing tip (i.e., tangent) of conispirals, or conical helices. The distinction
 175 between fixed- (conispiral and conihelical) and moving-frame (differential geometric)
 176 parameterizations, thus, begins to blur.

177 Another defining feature of fixed-frame models is, for obvious reasons, the fixed coiling
 178 axis. Rate of change in the direction of local coiling, $\hat{\mathbf{u}}$, is given by $\hat{\mathbf{u}}' = \mathbf{w} \times \hat{\mathbf{u}} =$
 179 $u\hat{\mathbf{u}} \times \hat{\mathbf{u}} + \lambda'\hat{\mathbf{n}} \times \hat{\mathbf{u}} = \lambda'\hat{\mathbf{n}} \times \hat{\mathbf{u}}$. In conihelical shells $\lambda' = 0$, and the Darboux vector, \mathbf{u} , defines the
 180 fixed coiling axis. Thus, given starting coiling direction (initial condition), conispiral coiling
 181 can be defined by apical and spiral angles, by lead angle and expansion rate, by lead angle
 182 and standardized local coiling, \tilde{u} , or by [Okamoto](#)’s standardized curvature and torsion. In all
 183 four cases, if parameter values remain fixed, the initial coiling direction is maintained ($\hat{\mathbf{u}}' = 0$),
 184 becoming a fixed axis, and self-similar conispiral shells result. That is another metric by
 185 which the distinction between fixed- and moving-frame parametrizations seems superfluous.

186 Irregular coiling, allometry, or other deviations from self-similar conihelical geometry,
 187 always require a change in parameter values (notably, lead angle). Gradual rotation of the

188 local coiling axis, $\hat{\mathbf{u}}$, thus, occurs simultaneously with (transient) change in lead angle
 189 ($\lambda' \neq 0$), and by precessing around the vector of global coiling, \mathbf{w} (Fig. 1G). That is, in fact,
 190 another direct consequence of conihelical geometry; this time, prescribing a testable
 191 hypothesis on how shell geometry can deviate from isometric conihelical. Some evidence in
 192 support of this hypothesis appears in Ackerly's (1989b) visual and stereographical analyses
 193 of *Vermicularia*, which possesses a tightly coiled conspiral juvenile phase, followed by an
 194 open-coiled geometry that differs in both coiling axis and lead angle. Similarly, his analysis
 195 of *Distorsio* shows that lead angle varies among consecutive episodic growth increments,
 196 while the coiling axis precesses with an angular radius of roughly four to seven degrees.
 197 Savazzi (1996) provides examples from several species of *Tenagodus* (syn. *Siliquaria*) and
 198 *Vermicularia* that follow the same rule of simultaneous change in coiling axis and in lead
 199 angle. Particularly extreme cases occur in microsnaills (Clements *et al.* 2008; Liew *et al.* 2014)
 200 and in irregularly coiled (heteromorph) ammonoids (Okamoto 1988, 1996).

201 Initially, the allometric logarithmic helicospiral ($\gamma_z \neq \gamma_r$) seems to contradict the
 202 hypothesis, as lead angle increases ($\gamma_z > \gamma_r$) or decreases ($\gamma_z < \gamma_r$), while the coiling axis
 203 remains fixed. Similarly, in Harary & Tal's (2011)'s 'natural 3D spiral', lead angle varies
 204 smoothly between a starting value, λ_0 , and an asymptotic value, λ_∞ , at large arclengths;
 205 essentially, converging to a conspiral (though adult size and shape may be obtained well
 206 before that asymptote is reached). However, when the direction of $\mathbf{w} = u\hat{\mathbf{u}} + \lambda'\hat{\mathbf{h}}$ does not
 207 change, it acts as the new fixed coiling axis of the shell; its magnitude, $w = \sqrt{u^2 + (\lambda')^2}$, is the
 208 coiling rate around that axis (i.e., revolution angle per unit growth of centerline arclength,
 209 $d\theta/ds = w = \|\mathbf{w}\|$). This precession of the local moving Frenet frame around a potentially
 210 fixed axis, $\hat{\mathbf{w}}$, is another reason why fixed- and moving-frame models should be considered in
 211 tandem, as complementary points of view.

212 The condition of fixed $\hat{\mathbf{w}}$ is satisfied, for example, when local coiling and change in lead
 213 angle are both constant, $u = \text{const}$, $\lambda' = \text{const}$. These are the 'modulated curves' of Nutbourne
 214 & Martin (1988), better known as 'curves of constant precession' (Scofield 1995). Another
 215 class of curves, in which $\hat{\mathbf{w}}$ is fixed, are the already familiar conical and generalized helices.

216 This is just the degenerate case of $\mathbf{w} = \mathbf{u}$ and $\lambda' = 0$, where the precession vanishes.
 217 Extrapolating from both curves of constant precession and curves of constant slope
 218 (generalized helices), one obtains a class of curves called *slant helices* that includes the
 219 former two as special cases. A necessary and sufficient condition for a slant helix, in the
 220 notation of this study, is $\lambda' \propto u$, or $\lambda' = \sigma u$ where $\sigma = \text{const}$ (Izumiya & Takeuchi 2004 ; SI).

221 We can proceed still one step further and define the *logarithmic slant helix*, $u, \lambda' \propto 1/s$, or
 222 $u = \tilde{u}/s$ and $\lambda' = \sigma \tilde{u}/s$, where σ and \tilde{u} are constants (SI). While the logarithmic slant helix
 223 describes an allometrically growing shell, it does share some properties with the isometric
 224 conical helix. For example, revolution angle and arclength are similarly related through
 225 $\theta \propto \ln(s/s_0)$, and therefore arclength expands exponentially, $s = s_0 e^{\gamma_s \theta}$, where $\gamma_s = 1/\tilde{w}$,
 226 $\tilde{w} = \tilde{u}\sqrt{1 + \sigma^2}$. Another feature of logarithmic slant helices is that lead angle grows linearly
 227 with θ . Consecutive whorls, separated by a full revolution around the coiling axis ($\Delta\theta = 2\pi$),
 228 are always tilted relative to each other by the same amount, $\Delta\lambda = 2\pi\lambda'/w = 2\pi\sigma/\sqrt{1 + \sigma^2}$
 229 (Fig. 1H).

230 The logarithmic slant helix, thus, is a natural allometric extension of the isometric conical
 231 helix, in the sense that, instead of being fixed on the same initial value (λ_0) throughout
 232 ontogeny, lead angle grows linearly (i.e., $\lambda(\theta) = \lambda_0 + c\theta$; $c = \text{const}$). In that respect, it is the
 233 simplest case of centerline allometry, and provides insight into the more complex variation in
 234 other models (helicospirals, $\gamma_z \neq \gamma_r$, or Harary & Tal 2011). Clearly, lead angle cannot grow
 235 indefinitely, unless coiling becomes open and irregular. But, in any case, real shells have a
 236 finite number of whorls, and therefore, the logarithmic slant helix, like its older cousin, the
 237 conical helix, is a useful approximation. In particular, given expressions for the centerline
 238 curve, $x(\theta)$, $y(\theta)$, and $z(\theta)$ (SI), one can simulate such shells graphically (Fig. 1H,I).

239 **Supplementary information**

240 Additional derivations, explanations, methods, and discussion are in the supplementary
241 information document.

242 **DATA AND SOFTWARE AVAILABILITY.** All data and code are available at
243 <https://doi.org/10.5281/zenodo.19763621>, for the data analyses (Fig. 2), and at
244 <https://doi.org/10.5281/zenodo.19895626>, for the WebGL application of theoretical
245 morphology of coiled shells (Fig. 1).

246 **References**

- 247 Ackerly SC (1989a). Kinematics of accretionary shell growth, with examples from
248 brachiopods and molluscs. *Paleobiology* 15: 147–164. [10.1017/s0094837300009337](https://doi.org/10.1017/s0094837300009337).
- 249 Ackerly SC (1989b). Shell coiling in gastropods; analysis by stereographic projection.
250 *PALAIOS* 4: 374–378. [10.2307/3514561](https://doi.org/10.2307/3514561).
- 251 Araki A, Noshita K (2023). Theoretical morphological analysis of differential morphospace
252 occupation patterns for terrestrial and aquatic gastropods. *Evolution* 77: 1864–1873.
253 <https://doi.org/10.1093/evolut/qpad110>.
- 254 Archibald RC (1918). The logarithmic spiral (undergraduate mathematics clubs, topics for
255 club programs). *American Mathematical Monthly* 25: 189–193.
- 256 Bayer U (1978). Morphogenetic programs, instabilities, and evolution — a theoretical study.
257 *Neues Jahrb Geol Paläont Abh* 156: 226–261.
- 258 Béguinot J (2021). Adult shell-size regulation in conispirally-coiled shells: evidence for a
259 widespread negative covariance between whorls growth-rate and the final number of
260 whorls in land snails. *Annual Research & Review in Biology* 36: 95–106.
261 <https://doi.org/10.9734/arrb/2021/v36i1030439>.
- 262 Cain AJ (1980). Whorl number, shape, and size of shell in some pulmonate faunas. *J Conchol*
263 30: 209–221.
- 264 Cameron RAD (1981). Functional aspects of shell geometry in some british land snails. *Biol J*

265 *Linn Soc* 16: 157–167. <https://doi.org/10.1111/j.1095-8312.1981.tb01648.x>.

266 Chouaieb N, Goriely A, Maddocks JH (2006). Helices. *Proc Natl Acad Sci USA* 103: 9398–9403.
267 <https://doi.org/10.1073/pnas.0508370103>.

268 Clarke RK, Grahame J, Mill PJ (1999). Variation and constraint in the shells of two sibling
269 species of intertidal rough periwinkles (Gastropoda: *Littorina* spp.). *J Zool* 247: 145–154.
270 [10.1111/j.1469-7998.1999.tb00978.x](https://doi.org/10.1111/j.1469-7998.1999.tb00978.x).

271 Clements R, Liew TS, Vermeulen JJ, Schilthuizen M (2008). Further twists in gastropod shell
272 evolution. *Biology Letters* 4: 179 – 182. <https://doi.org/10.1098/rsbl.2007.0602>.

273 Cortie M (1989). Models for mollusc shell shape. *South African Journal of Science* 85: 454–460.

274 Ekaratne SUK, Crisp DJ (1983). A geometric analysis of growth in gastropod shells, with
275 particular reference to turbinate forms. *Journal of Marine Biology Association UK* 63:
276 777–797.

277 Fowler DR, Meinhardt H, Prusinkiewicz P (1992). Modeling seashells. *Proceedings of the 19th*
278 *annual conference on Computer graphics and interactive techniques*, pp. 379–387.
279 [10.1145/133994.134096](https://doi.org/10.1145/133994.134096).

280 Frýda J, Ferrová L (2011). The oldest evidence of non-coaxial shell heterostrophy in the class
281 Gastropoda. *Bull Geosci* 86: 765–776. [10.3140/bull.geosci.1302](https://doi.org/10.3140/bull.geosci.1302).

282 Gerber S (2017). The geometry of morphospaces: lessons from the classic Raup shell coiling
283 model. *Biol Rev* 92: 1142–1155. <https://doi.org/10.1111/brv.12276>.

284 Goriely A (2017). *The Mathematics and Mechanics of Biological Growth*. Springer.
285 <https://doi.org/10.1007/978-0-387-87710-5>.

286 Gould SJ (1989). A developmental constraint in *Cerion*, with comments on the definition and
287 interpretation of constraint in evolution. *Evolution* 43: 516–539.

288 Güzelkardeşler G, Şahiner B (2024). An alternative approach to find the position vector of a
289 general helix. *Celal Bayar University Journal of Science* 20: 54–60.
290 [10.18466/cbayarfbe.1479066](https://doi.org/10.18466/cbayarfbe.1479066).

291 Hammer Ø (2016). *Perfect Shape: Spiral Stories*. Springer.

- 292 Harary G, Tal A (2011). The natural 3d spiral. *Computer Graphics Forum* 30: 237–246.
293 <https://doi.org/10.1111/j.1467-8659.2011.01855.x>.
- 294 Hutchinson JMC (1989). Control of gastropod shell shape: the role of the preceding whorl. *J*
295 *Theor Biol* 140: 431–444.
- 296 Hutchinson JMC (1990). Control of gastropod shell form via aperture growth rates. *J*
297 *Morphol* 206: 259–264.
- 298 Illert C (1983). The mathematics of gnomonic seashells. *Math Biosci* 63: 21–56.
- 299 Izumiya S, Takeuchi N (2004). New special curves and developable surfaces. *Turkish Journal*
300 *of Mathematics* 28: 153–164.
- 301 Kohn AJ, Riggs AC (1975). Morphometry of the *Conus* shell. *Syst Zool* 24: 346–359.
- 302 Larsson J, Westram AM, Bengmark S, Lundh T, Butlin RK, Butlin RK (2020). A
303 developmentally descriptive method for quantifying shape in gastropod shells. *J R Soc*
304 *Interface* 17. <http://dx.doi.org/10.1098/rsif.2019.0721>.
- 305 Liew TS, Kok ACM, Schilthuizen M, Urdy S (2014). On growth and form of irregular
306 coiled-shell of a terrestrial snail: *Plectostoma concinnum* (Fulton, 1901) (Mollusca:
307 Caenogastropoda: Diplommatinidae). *PeerJ* 2: e383.
308 <https://doi.org/10.7717/peerj.383>.
- 309 Liew TS, Schilthuizen M (2016). A method for quantifying, visualising, and analysing
310 gastropod shell form. *PLOS ONE* 11: 1–24.
311 <https://doi.org/10.1371/journal.pone.0157069>.
- 312 Løvtrup S, Løvtrup M (1988). The morphogenesis of molluscan shells: a mathematical
313 account using biological parameters. *J Morphol* 197: 53–62.
- 314 Løvtrup S, von Sydow B (1974). D’arcy Thompson’s theorem and the shape of the molluscan
315 shell. *Bull Math Biol* 36: 567–575.
- 316 McGhee GR (1978). Analysis of the shell torsion phenomenon in the Bivalvia. *Lethaia* 11:
317 315–329. <https://doi.org/10.1111/j.1502-3931.1978.tb01889.x>.
- 318 McGhee GR (1999). *Theoretical Morphology: The Concept and Its Applications*. Perspectives in

319 Earth History and Paleobiology. Columbia University Press, New York.

320 Monnet C, Zollikofer C, Bucher H, Goudemand N (2009). Three-dimensional morphometric
321 ontogeny of mollusc shells by micro-computed tomography and geometric analysis.
322 *Palaeontol Electron* 12: 1–13. <https://doi.org/10.5167/uzh-23587>.

323 Moseley H (1838). On the geometrical forms of turbinated and discoid shells. *Philosophical*
324 *Transactions of the Royal Society of London* 1838: 351–370.

325 Moseley H (1842). On conchylometry. *Lond Edinb Dubl Phil Mag* 21: 300–305.

326 Moulton D, Goriely A, Chirat R (2012). Mechanical growth and morphogenesis of seashells. *J*
327 *Theor Biol* 311: 69–79. <https://doi.org/10.1016/j.jtbi.2012.07.009>.

328 Moulton DE, Goriely A (2012). Surface growth kinematics via local curve evolution. *J of*
329 *Math Biol* 68: 81–108.

330 Naumann CF (1845). Über die wahre Spirale der Ammoniten. *Annalen der Physik* 140:
331 538–543. <https://doi.org/10.1002/andp.18451400406>.

332 Newkirk GF, Doyle RW (1975). Genetic analysis of shell-shape variation in *Littorina saxatilis*
333 on an environmental cline. *Mar Biol* 30: 227–237. [10.1007/BF00390745](https://doi.org/10.1007/BF00390745).

334 Noshita K (2014). Quantification and geometric analysis of coiling patterns in gastropod
335 shells based on 3d and 2d image data. *J Theor Biol* 363: 93–104.

336 Noshita K, Asami T, Ubukata T (2012). Functional constraints on coiling geometry and
337 aperture inclination in gastropods. *Paleobiology* 38: 322–334. [10.1666/10060.1](https://doi.org/10.1666/10060.1).

338 Noshita K, Shimizu K, Sasaki T (2016). Geometric analysis and estimation of the growth rate
339 gradient on gastropod shells. *J Theor Biol* 389: 11–19.
340 <https://api.semanticscholar.org/CorpusID:39448122>.

341 Nutbourne AW, Martin RR (1988). *Differential geometry applied to curve and surface design:*
342 *Foundations*. Ellis Horwood, Chichester, England.

343 Okabe T, Yoshimura J (2017). Optimal designs of mollusk shells from bivalves to snails.
344 *Scientific Reports* 7: 42445. <https://doi.org/10.1038/srep42445>.

345 Okamoto T (1988). Analysis of heteromorph ammonoids by differential geometry.

346 *Paleobiology* 31: 35–52.

347 Okamoto T (1996). Theoretical modeling of ammonoid morphology. In *Ammonoid*
348 *Paleobiology* (edited by Landman NH, Tanabe K, Davis RA), pp. 225–251. Springer US,
349 Boston, MA. https://doi.org/10.1007/978-1-4757-9153-2_8.

350 Páll-Gergely B, Sipos AÁ, Harzhauser M, Örstan A, Winkler V, Neubauer TA (2024). Many
351 roads to success: alternative routes to building an economic shell in land snails. *Evolution*
352 78: 778–786. <https://doi.org/10.1093/evolut/qpae018>.

353 Raup DM (1961). The geometry of coiling in gastropods. *Proc Natl Acad Sci USA* 47: 602–609.
354 <https://doi.org/10.1073/pnas.47.4.602>.

355 Raup DM (1966). Geometric analysis of shell coiling: general problems. *J Paleontol* 40:
356 1178–1190.

357 Raup DM (1967). Geometric analysis of shell coiling: coiling in ammonoids. *J Paleontol* 41:
358 43–65.

359 Raup DM, Graus RR (1972). General equations for volume and surface area of a
360 logarithmically coiled shell. *Mathematical Geology* 4: 307–316.

361 Raup DM, Michelson A (1965). Theoretical morphology of the coiled shell. *Science* 147:
362 1294–1295.

363 Rice SH (1998). The bio-geometry of mollusc shells. *Paleobiology* 24: 133–149.

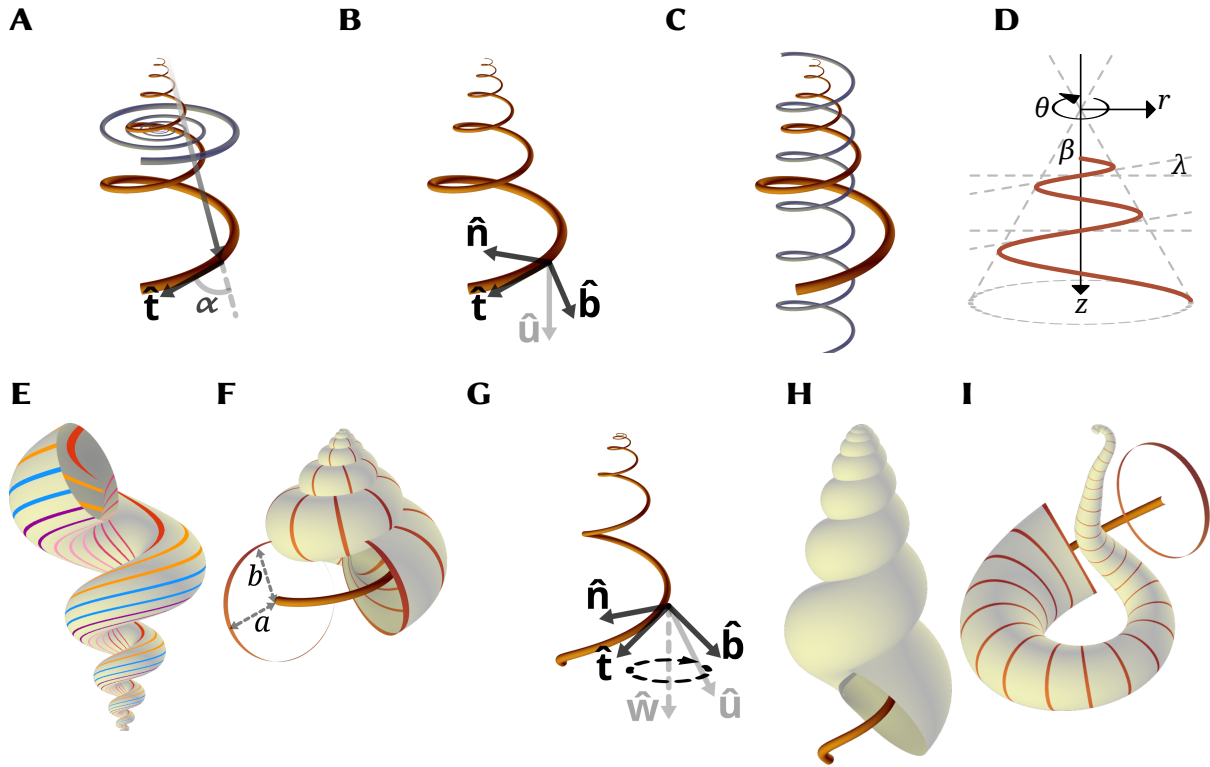
364 Savazzi E (1990). Biological aspects of theoretical shell morphology. *Lethaia* 23: 195–212.

365 Savazzi E (1996). Adaptations of vermetid and silicuarid gastropods. *Palaeontology* 39:
366 157–177.

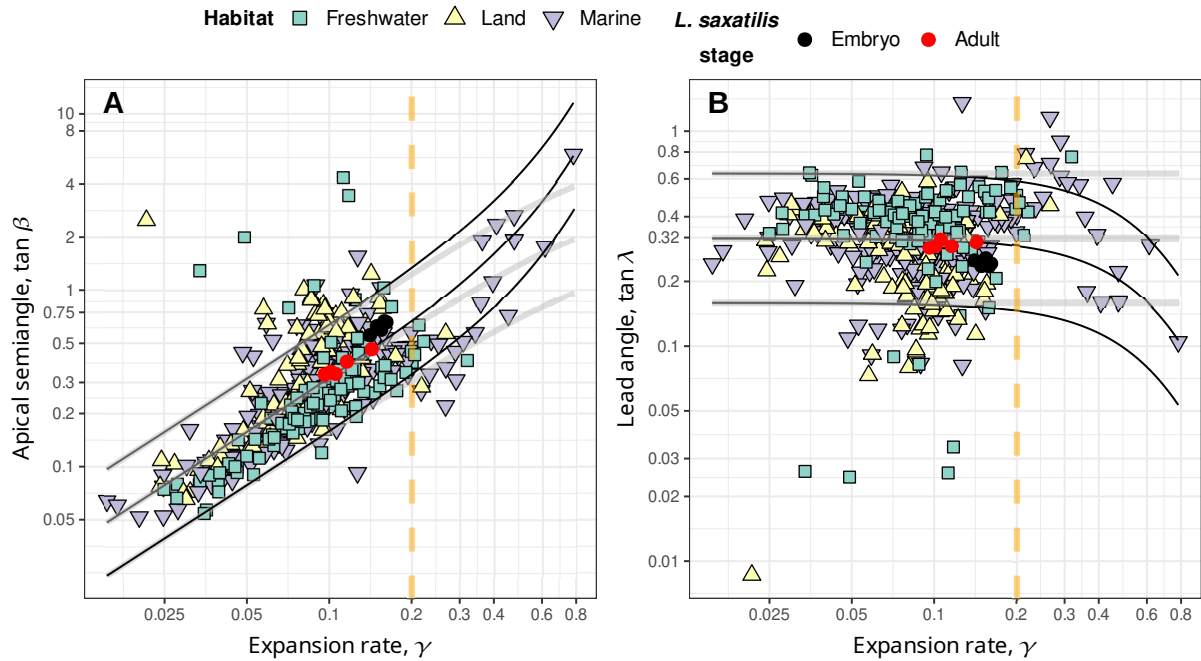
367 Schindel DE (1990). Unoccupied morphospace and the coiled geometry of gastropods:
368 architectural constraint or geometric covariation? In *Causes of Evolution: a paleontological*
369 *perspective* (edited by Ross R, Allmon W), pp. 270–304. University of Chicago Press,
370 Chicago.

371 Scofield PD (1995). Curves of constant precession. *The American Mathematical Monthly* 102:
372 531–537. <https://doi.org/10.1080/00029890.1995.12004613>.

- 373 Stone JR (1995). CerioShell: a computer program designed to simulate variation in shell form.
374 *Paleobiology* 21: 509–519.
- 375 Swan ARH (2015). Heterochrony in helicoid spiral cones: a computer model for
376 demonstrating heterochronic evolution. *Palaeontol Electron* 18: 1–11. [10.26879/510](https://doi.org/10.26879/510).
- 377 Thompson DW ([1942] 1992). *On Growth and Form: The Complete Revised Edition*. Dover,
378 New York.
- 379 Tursch B (1997). Spiral growth: The ‘Museum of all shells’ revisited. *J Molluscan Stud* 63:
380 547–554. <https://doi.org/10.1093/mollus/63.4.547>.
- 381 Urdy S, Goudemand N, Bucher H, Chirat R (2010). Allometries and the morphogenesis of the
382 molluscan shell: a quantitative and theoretical model. *J Exp Zool* 314B: 280–302.
383 [10.1002/jez.b.21337](https://doi.org/10.1002/jez.b.21337).
- 384 Uzunoğlu B, İsmail Gök, Yaylı Y (2016). A new approach on curves of constant precession.
385 *Applied Mathematics and Computation* 275: 317–323.
386 <https://doi.org/10.1016/j.amc.2015.11.083>.
- 387 van Osselaer C, Grosjean P (2000). Suture and location of the coiling axis in gastropod shells.
388 *Paleobiology* 26: 238–257.
389 [https://doi.org/10.1666/0094-8373\(2000\)026<0238:SAL0TC>2.0.CO;2](https://doi.org/10.1666/0094-8373(2000)026<0238:SAL0TC>2.0.CO;2).
- 390 Vermeij GJ (2002). Characters in context: molluscan shells and the forces that mold them.
391 *Paleobiology* 28: 41–54.
- 392 Vinarski MV (2014). The birth of malacology. when and how? *Zoosystematics and Evolution*
393 90: 1–5.



394 Figure 1 : Theoretical morphology in a snailshell. (A,B,C) Three parameterizations of conical logspirals; re-
 395 spectively conispiral, differential geometric, and conihelical. (A) Constant spiral angle, α , between instantaneous
 396 tangent vector, $\hat{\mathbf{t}}$, and radius-vector from pole (apex) defines the conispiral parameterization. The conispiral is
 397 as if a corresponding logarithmic base planispiral (in blue), with same expansion rate, γ , has been stretched out
 398 of its plane, to form a three-dimensional space curve. (B) The differential geometric parameterization follows
 399 the evolution of the Frenet moving frame, defined by tangent $\hat{\mathbf{t}}$, principal normal, $\hat{\mathbf{n}}$, and binormal, $\hat{\mathbf{b}} = \hat{\mathbf{t}} \times \hat{\mathbf{n}}$.
 400 The frame's rotation is defined by the Darboux vector $\mathbf{u} = u\hat{\mathbf{u}} = \tau\hat{\mathbf{t}} + \kappa\hat{\mathbf{b}} = u \sin \lambda \hat{\mathbf{t}} + u \cos \lambda \hat{\mathbf{b}}$; κ is curvature, and τ
 401 torsion (SI). (C) In the conihelical parameterization, a conical logspiral is viewed as a helix with expanding radius
 402 — a conical helix. For comparison, a circular helix with same slope (i.e., lead angle) is also illustrated. (D) Coni-
 403 cal helix in side view. Apical semiangle, β , lead angle, λ , and the cylindrical coordinate system illustrated. The
 404 z -direction coincides with the coiling axis. (E) Multispiral approach to shell modeling, where shell surface is
 405 defined by many spiral paths, differing in lead angle. For illustration purposes, an exaggerated open-coiled shell
 406 is shown, where slopes of inner spirals are clearly steeper. Nevertheless, all spirals share the same expansion
 407 rate, γ . (F) Generating curve approach to shell modeling. Shell surface defined by a closed figure (here a circle)
 408 that sweeps along a conihelical centerline. Also illustrated are the size measures, a and b (not to be confused
 409 with the binormal vector, $\hat{\mathbf{b}}$), roughly corresponding respectively to aperture size perpendicular and parallel to
 410 the coiling axis. (G) In allometric shells, where centerline's lead angle varies, the Darboux vector is no longer
 411 fixed, but precesses around an axis $\mathbf{w} = w\hat{\mathbf{w}}$ that contains a λ' component (Eq.[3]; SI). (H,I) Allometric and irreg-
 412 ularly coiled shells with logarithmic slant helix centerline. Lead angles are initially 0 (i.e., planispiral coiling), but
 413 subsequently grow at different rates. Parameters values to simulate all shell images of this figure in the WebGL
 414 application are provided in SI.



416 Figure 2 : Apical semiangle, as $\tan \beta$ (panel A), and lead angle, as $\tan \lambda$ (panel B), against expansion rate,
 417 $\gamma = \ln W / 2\pi$, from the data in Noshita *et al.* (2012) and Araki & Noshita (2023) on coiling parameters of over 400
 418 species of freshwater, marine, and terrestrial gastropods, and the data of Newkirk & Doyle (1975) on embryos and
 419 adults of *Littorina saxatilis* from five different populations in Nova Scotia. In both panels, a vertical dashed line for
 420 $\gamma = 0.2$ marks roughly the domain of validity for small- γ approximations (SI), where nevertheless most data lies.
 421 Illustrated curves, however, were drawn using full (exact, non-approximate) expressions (SI). (A) When apical
 422 semiangle is plotted against expansion rate, a clear linear trend is visible. Solid black lines indicate boundaries
 423 for whorl-overlap, $\tan \beta > (1/\rho) \sinh(\pi\gamma)$, for $\rho = 0.5, 1, 2$ (upper to lower; where ρ is defined as $\rho = b/a$, ratio
 424 of aperture sizes, as illustrated in Fig. 1F; $\rho = 1$ means a circular aperture) that separates tightly-coiled (above
 425 boundary line) and open-coiled shells (below boundary line). In the range $\gamma \leq 0.2$, such boundary curves for tight-
 426 coiling, however, are practically indistinguishable from relationships that fixed lead angles in Eq.[2] prescribe
 427 ($\tan \beta = \left(\gamma / \sqrt{1 + \gamma^2} \right) \cot \lambda$; gray lines), given $\tan \lambda = \rho / \pi$ (SI; $D = 0$ for illustrated curves; i.e., apertures touching
 428 the coiling axis). Raw values for apical angles were transformed to correspond to centerlines by doubling reported
 429 values of T . (B) Estimates of lead angle, $\tan \lambda$, obtained from Eq.[2]. Compared to panel A, there is clearly less
 430 variation in lead angle than in apical angle, and the linear trend disappears; suggesting independent variation in
 431 expansion rate, γ , and lead angle, λ . Black and gray solid curves correspond to those in panel A, but in reverse
 432 order ($\rho = 2, 1, 0.5$, upper to lower respectively).

415

433

S1 **Supplementary information for “Lead and slant on the geometry of**
S2 **coiling in gastropods”**

S3

S4 Ido Filin ¹ *

S5 ¹ No author affiliation.

S6 * Corresponding author. E-mail: ido@filin.fi

S7

S8 **Contents**

| | | |
|-----|--|-----------|
| S9 | S1 A note on terminology and notation | 2 |
| S10 | S2 Expressions for logarithmic conispirals | 3 |
| S11 | S3 Whorl-overlap condition for non-circular and displaced generating curves | 4 |
| S12 | S4 Approximation errors | 6 |
| S13 | S5 Differential geometric parameterization | 6 |
| S14 | S6 Logarithmic slant helix | 9 |
| S15 | S7 Web application | 10 |
| S16 | S8 Supplementary references | 10 |

S17 **S1 A note on terminology and notation**

S18 [Thompson \(\[1942\] 1992\)](#) defined three angles, related to the modeling of equiangular (i.e.,
S19 logarithmic) spiral shells. The spiral angle, α , is the angle between the radius-vector from the
S20 pole (or apex of the conical envelope) and the tangent to the spiral. His β denotes the apical
S21 semiangle, as in this study. His γ refers to the “angle of retardation”, relevant when
S22 considering the inner and outer margins of planispiral shells. Given that the angle of
S23 retardation has been rarely utilized since, I reclaim the symbol γ for denoting the
S24 exponential expansion rate in this study.

S25 Generalized or general helices ([Nutbourne & Martin 1988](#)) are defined by the constant
S26 slope, relative to a fixed direction. Hence, the alternative term, curve of constant slope
S27 ([Scofield 1995](#)). Somewhat confusingly they are also often called ‘cylindrical helices’ ([O’Neill](#)
S28 [2006](#)), referring to a generalized cylinder. But I avoid this term here.

S29 While ‘pitch’ is used often with circular helices to refer to the slope of the helix (e.g.,
S30 [Chouaieb et al. 2006](#)), strictly speaking, pitch is the distance between adjacent threads or
S31 strands. Lead, on the other hand, is the axial progression per one full revolution of the helical
S32 structure, which is the quantity of interest in this study. Lead and pitch are the same for
S33 single-thread helices, but not for double or triple helices, such as in double- and multi-start
S34 screws and various helical structures in biology.

S35 The slope of the helix, $\tan \lambda$, can be measured by the lead angle, as in this study, by the
S36 ‘helix slope’ itself (e.g., [De Renzi & Mayoral 2024](#); also ‘rise’, [Hauser et al. 2017](#)), or by the
S37 ‘helix angle’, relative to the fixed axis (the complementary angle to the lead angle; [Nutbourne](#)
S38 [& Martin 1988](#)). The latter was referred to as ‘inclination angle’ by [Moseley \(1842\)](#), in his
S39 work on conchylometry. However, more recently, inclination angle is used to describe the
S40 orientation of the aperture itself relative to the coiling axis ([Schindel 1990](#); [Vermeij 1993](#);
S41 [Noshita et al. 2012](#)), so I avoid this term here.

S42 Finally, the quantity $u = \sqrt{\kappa^2 + \tau^2}$, which is the norm of the Darboux vector, where κ is
S43 curvature and τ is torsion, does not have a standard name. [Nutbourne & Martin \(1988\)](#) refer

S44 to it as ‘compound curvature’, and Güzelkardeşler & Şahiner (2024) call it ‘first alternative
S45 curvatrue’. Other appropriate terms may be ‘winding’ or ‘twist’, in reference to circular
S46 helices (Chouaieb *et al.* 2006; Goriely 2017). But those usually involve additional meaning in
S47 terms of mechanical properties. It is also sometimes called angular rate, speed, or velocity,
S48 though time is only implicit here, and u measures rotation angle per unit arclength, not time.
S49 In this study, I refer to the Darboux vector and its norm, as well as to \mathbf{w} and w , simply as
S50 vectors and rates of coiling, as in the end, they describe direction and rate of rotation. While
S51 the greek letter ω is often used to denote the Darboux vector and $\sqrt{\kappa^2 + \tau^2}$ (Nutbourne &
S52 Martin 1988), I avoid this notation, so not to confuse with true angular velocity in mechanics.

S53 S2 Expressions for logarithmic conispirals

S54 Eq.[1] of the main text, $\cot \alpha \sin \beta = \gamma$, has been derived and used enough times, so not to
S55 require any explanation (Moseley 1842; Thompson [1942] 1992; Raup & Graus 1972; Løvtrup
S56 & von Sydow 1974; Ekaratne & Crisp 1983; Illert 1983). From geometry of cones, it is easy to
S57 see that

$$S58 \quad \sin \lambda = \cos \alpha \cos \beta \quad (S1)$$

S59 (Moseley 1842; up to differences in notation and definition of lead angle), the expression for
S60 spiral height dilation, q_z . These two equations can be combined to produce

$$S61 \quad \tan \lambda \tan \beta = \frac{\gamma}{\sqrt{1 + \gamma^2}}. \quad (S2)$$

S62 Values of γ for gastropods are typically below 0.2 (Thompson [1942] 1992; Cameron 1981;
S63 Fig. 3), corresponding to relatively slower expansion and shells that exhibit several complete
S64 whorls. For small values of γ , Eq.[S2] is approximated by Eq.[2] of the main text.

S65 The expression for a conispiral shell’s height-to-arclength ratio, derived by Ekaratne &
S66 Crisp (1983), can be written as $(z + b)/s$ in this study, which translates to $q_z + q_b = \sin \lambda + q_b$.
S67 Alternatively, using the steps of their derivation and following the suture spiral on the outer
S68 surface of the shell, rather than the centerline spiral, $(z/W + 2b)/s = (1/W) \sin \lambda + (2\rho a/s) =$
S69 $(1/W) \sin \lambda + \rho r/s = \sin \lambda(1/W + \rho \tan \beta)$ (where s , r , λ and β all refer now to the suture
S70 spiral, W is the whorl expansion rate [Eq.[S3] below], and using the relations $\rho = b/a$, $r = 2a$,

S71 and $r = z \tan \beta = s \sin \lambda \tan \beta$). In any case, all these ratios are constants for self-similar
S72 logarithmic conispiral shells.

S73 **S3 Whorl-overlap condition for non-circular and displaced generating curves**

S74 Mathematical and computational shell modeling got a boost with the work of David Raup in
S75 the 1960s (Raup 1961; Raup & Michelson 1965; Raup 1966) that also kick-started theoretical
S76 morphology. Raup's model for gastropod shell coiling (Raup 1961, 1966; Raup & Michelson
S77 1965) contains four parameters that are designed to be estimated from sagittal cross-sections
S78 of shells. His whorl expansion rate, W , is related to γ through

$$S79 \quad W = e^{2\pi\gamma}. \quad (S3)$$

S80 His translation rate, T , is related to β by

$$S81 \quad T = \cot \beta. \quad (S4)$$

S82 The *displacement* parameter (Schindel 1990), D , measures relative distance of the aperture
S83 from the coiling axis, and is given by

$$S84 \quad D = \frac{r - a}{r + a}, \quad (S5)$$

S85 where a is aperture size in the r -direction (i.e., half the aperture's width in the r -direction).

S86 The umbilicus (or columellar) radius, ξ , i.e., distance of innermost aperture margin to the
S87 coiling axis, and the aperture size, a , are then given by

$$S88 \quad \begin{aligned} a &= \left(\frac{1-D}{1+D}\right) r, \\ \xi &= r - a = \left(\frac{2D}{1+D}\right) r. \end{aligned} \quad (S6)$$

S89 Raup's fourth parameter, S , broadly defines the shape of the generating curve, and is never
S90 really defined in his formulation. In principle, it may be vector- or function-valued, e.g.,
S91 $S = S(\varphi)$ (φ being some parameterization of the generating curve). It is, however, very often
S92 taken to be some ratio of major and minor axes of an ellipse — a natural extension of the
S93 circular generating curve (Raup 1966; Kohn & Riggs 1975; Newkirk & Doyle 1975; McNair
S94 *et al.* 1981; Ekaratne & Crisp 1983; Kemp & Bertness 1984; Ackerly 1992; Stone 1995; McGhee

S95 1999; Clarke *et al.* 1999; Urdy *et al.* 2010; Larsson *et al.* 2020). Here, I follow Ekaratne & Crisp
S96 (1983) and define aperture size a , perpendicular to the coiling axis, and aperture size b ,
S97 parallel to the axis, as illustrated in Fig. 1F of main text.

S98 The centers of two consecutive whorls (separated by $\Delta\theta = 2\pi$) are at distances r and rW
S99 from the coiling axis. Their distances to the apex are $r\sqrt{1+T^2}$ and $rW\sqrt{1+T^2}$, respectively.
S100 Aperture sizes along the conical envelope of the centerline spiral, i.e., at angle β to the coiling
S101 axis, are given by the radii of the elliptic generating curves at that angle $\frac{\rho a}{\sqrt{\rho^2 \sin^2 \beta + \cos^2 \beta}}$ and
S102 $\frac{\rho a W}{\sqrt{\rho^2 \sin^2 \beta + \cos^2 \beta}}$ respectively, where $\rho = b/a$. The whorl overlap condition is therefore,

$$S103 \quad r(W-1)\sqrt{1+T^2} < \frac{a\rho(W+1)\sqrt{1+T^2}}{\sqrt{\rho^2+T^2}}. \quad (S7)$$

S104 (recall that $T = \cot \beta$, and so $\sin^2 \beta = \frac{1}{1+T^2}$ and $\cos^2 \beta = \frac{T^2}{1+T^2}$). Substituting the expression for
S105 a from Eq.[S6], and further trivial manipulations give

$$S106 \quad T^2 < \rho^2 \left(\frac{\left(\frac{1-D}{1+D}\right)^2 (W+1)^2 - (W-1)^2}{(W-1)^2} \right), \quad (S8)$$

S107 or

$$S108 \quad T^2 < \rho^2 \frac{4W + 4D^2W - 4DW^2 - 4D}{(1+D)^2(W-1)^2}. \quad (S9)$$

S109 For a circular aperture ($\rho = 1$) touching the coiling axis ($D = 0$), I obtain Raup's (1966)
S110 expression for the "univalve-bivalve" boundary, $T = \frac{2\sqrt{W}}{W-1}$, on the W - T face of his
S111 morphospace cube. Substituting $T = 0$ in Eq.[S7] gives the "univalve-bivalve" boundary on
S112 the W - D face, $D < 1/W$, which is Raup's (1966) whorl-overlap condition for planispiral
S113 shells.

S114 In terms of γ and β , Eq.[S8] can be rewritten as

$$S115 \quad \cot^2 \beta < \rho^2 \left(\left(\frac{1-D}{1+D} \right)^2 \coth^2(\pi\gamma) - 1 \right) = \rho^2 \left(\left(\frac{1-D}{1+D} \right)^2 \frac{1}{\sinh^2(\pi\gamma)} - \frac{4D}{(1+D)^2} \right) \quad (S10)$$

S116 or

$$S117 \quad \tan \beta > \frac{1+D}{\rho} \frac{\sinh(\pi\gamma)}{\sqrt{(1-D)^2 - 4D \sinh^2(\pi\gamma)}}. \quad (S11)$$

S118 For circular apertures ($a = b$; $\rho = 1$) and $D = 0$, this equation gives the expression of Raup's
S119 whorl-overlap boundary in terms of γ and β of this study, $\tan \beta = \sinh(\pi\gamma)$.

S120 From Eq.[S10] one can get the condition for whorl-overlap in terms of $\sin \beta$,

$$S121 \quad \sin^2 \beta > \frac{1}{\rho^2 \left(\frac{1-D}{1+D}\right)^2 \coth^2(\pi\gamma) + (1 - \rho^2)}. \quad (S12)$$

S122 For $D = 0$ this simplifies to

$$S123 \quad \sin^2 \beta > \frac{\sinh^2(\pi\gamma)}{\sinh^2(\pi\gamma) + \rho^2}. \quad (S13)$$

S124 For $D = 0$ and $\rho = 1$, the condition further reduces to $\sin \beta > \tanh \pi\gamma$, the expression arrived at
S125 by [Clarke et al. \(1999\)](#); after correcting their typo and accounting for difference in definition
S126 of apical semiangle).

S127 Combining Eq.[S11] and Eq.[S2], I get the whorl-overlap boundary in terms of lead angle,

$$S128 \quad \tan \lambda < \frac{\rho}{1+D} \frac{\gamma \sqrt{(1-D)^2 - 4D \sinh^2(\pi\gamma)}}{\sqrt{1 + \gamma^2} \sinh(\pi\gamma)}. \quad (S14)$$

S129 Applying the small- γ approximation, the whorl overlap condition for lead angle becomes

$$S130 \quad \tan \lambda < \left(\frac{1-D}{1+D}\right) \frac{\rho}{\pi} + \mathcal{O}(\gamma^2), \quad (S15)$$

S131 providing the corresponding fixed value of lead angle that matches the whorl overlap
S132 condition for particular aperture shape, ρ , and aperture displacement, D .

S133 **S4 Approximation errors**

S134 For the range of γ -values exhibited by most gastropods, $\gamma \leq 0.2$ ([Thompson \[1942\] 1992](#);
S135 [Cameron 1981](#)), the error between the full and approximate versions of Eq.[S2] (Eq.[2] in the
S136 main text) is no more than 2%. This is derived from the ratio of the right-hand-sides of Eq.[2]
S137 and Eq.[S2], $\sqrt{1 + \gamma^2}$, which clearly increases with γ , and is 1 for $\gamma = 0$ and 1.0198 for $\gamma = 0.2$.

S138 **S5 Differential geometric parameterization**

S139 The typical approach in differential geometry is to follow the Frenet frame, attached to a
S140 space curve; though other local (moving) frames are possible ([Moulton & Goriely 2012](#);
S141 [Moulton et al. 2012](#); [Uzunoğlu et al. 2016](#); [Goriely 2017](#); [Güzelkardeşler & Şahiner 2024](#) ; see
S142 below). The Frenet frame is composed of the tangent, principal normal, and binormal unit
S143 vectors of the space curve, $\hat{\mathbf{t}}$, $\hat{\mathbf{n}}$, and $\hat{\mathbf{b}}$, respectively, parameterized by arclength, s , along the

S144 curve. The frame changes along the curve according to the Frenet-Serret differential
 S145 equations,

$$\begin{aligned}\hat{\mathbf{t}}' &= \frac{d\hat{\mathbf{t}}}{ds} = \mathbf{u} \times \hat{\mathbf{t}} = \kappa \hat{\mathbf{n}} \\ \hat{\mathbf{n}}' &= \mathbf{u} \times \hat{\mathbf{n}} = \tau \hat{\mathbf{b}} - \kappa \hat{\mathbf{t}} \\ \hat{\mathbf{b}}' &= \mathbf{u} \times \hat{\mathbf{b}} = -\tau \hat{\mathbf{n}},\end{aligned}\tag{S16}$$

S147 where \times is vector cross-product in 3D Euclidean space, \mathbf{u} is the Darboux vector,

$$\mathbf{u} = u\hat{\mathbf{u}} = \tau\hat{\mathbf{t}} + \kappa\hat{\mathbf{b}},\tag{S17}$$

S149 u is the vector's magnitude (i.e., local coiling; or the compound curvature of [Nutbourne &](#)
 S150 [Martin 1988](#); see §S1), $\kappa = u \cos \lambda$ is curvature, and $\tau = u \sin \lambda$ is torsion. The Darboux vector,
 S151 thus, describes the instantaneous rotation of the Frenet moving-frame, with respect to
 S152 arclength (rather than time). For generalized helices ($\tau/\kappa = \tan \lambda = \text{const}$), including conical
 S153 helices, the direction of the Darboux vector is fixed, $\hat{\mathbf{u}}' = 0$, though coiling rate, u , itself can
 S154 change (e.g., for conical helices $u \propto 1/s$). In other words, for generalized helices $\mathbf{u}' = u'\hat{\mathbf{u}}$, and
 S155 the direction $\hat{\mathbf{u}}$ determines the fixed coiling axis of the helix.

S156 If lead angle changes with arclength, the space curve is no longer a generalized helix, and
 S157 the direction of \mathbf{u} changes along the curve, $\hat{\mathbf{u}}' \neq 0$ and $\mathbf{u}' = u'\hat{\mathbf{u}} + u\hat{\mathbf{u}}'$. Because $\hat{\mathbf{u}}$ is a unit
 S158 vector, its derivative can be written as a cross-product with some instantaneous rotation
 S159 vector, \mathbf{w} , such that $\hat{\mathbf{u}}' = \mathbf{w} \times \hat{\mathbf{u}}$. For generalized helices $\mathbf{w} \equiv \mathbf{u}$, and so $\hat{\mathbf{u}}' = \mathbf{u} \times \hat{\mathbf{u}} = u\hat{\mathbf{u}} \times \hat{\mathbf{u}} \equiv 0$.
 S160 In the general case, we write $\mathbf{w} = w_1\hat{\mathbf{t}} + w_2\hat{\mathbf{n}} + w_3\hat{\mathbf{b}}$, and attempt to find the w_i from
 S161 Eqs.[S16] and [S17].

S162 First, note that from Eq.[S17] $\hat{\mathbf{u}} = \hat{\mathbf{t}} \sin \lambda + \hat{\mathbf{b}} \cos \lambda$, and therefore by applying the
 S163 Frenet-Serret relations (Eq.[S16]), $\hat{\mathbf{u}}' = (\hat{\mathbf{t}} \cos \lambda - \hat{\mathbf{b}} \sin \lambda)\lambda'$. Expanding the rotation vector,
 S164 $\mathbf{w} \times \hat{\mathbf{u}} = (-w_2\hat{\mathbf{b}} + w_3\hat{\mathbf{n}}) \sin \lambda + (-w_1\hat{\mathbf{n}} + w_2\hat{\mathbf{t}}) \cos \lambda$. Equating the two expressions per
 S165 component, one obtains $w_2 = \lambda'$, and $w_3 = w_1 \cot \lambda$, while w_1 still remains unknown. We can
 S166 already guess, based on $\mathbf{w} = \mathbf{u}$ for generalized helices, that $w_1 = u \sin \lambda = \tau$ and
 S167 $w_3 = u \cos \lambda = \kappa$. That is corroborated by noting that the Darboux vector does not have a
 S168 $\hat{\mathbf{n}}$ -component, i.e., $\hat{\mathbf{u}}$ and $\hat{\mathbf{n}}$ are always perpendicular to each other. Consequently, we can
 S169 construct the alternative orthonormal moving-frame of [Uzunoğlu et al. \(2016\)](#) and

S170 [Güzelkardeşler & Şahiner \(2024\)](#), composed of $\hat{\mathbf{u}}$, $\hat{\mathbf{n}}$, and $\hat{\mathbf{u}} \times \hat{\mathbf{n}}$. The rotation vector of this
S171 frame is \mathbf{w} , resulting in the relation $\hat{\mathbf{n}}' = \mathbf{w} \times \hat{\mathbf{n}} = w_1 \hat{\mathbf{b}} - w_3 \hat{\mathbf{t}}$. But from the Frenet-Serret
S172 equations (Eq.[S16]) we know that $\hat{\mathbf{n}}' = \tau \hat{\mathbf{b}} - \kappa \hat{\mathbf{t}}$, and so $w_1 = \tau$ and $w_3 = \kappa$, or in vector form,

$$\begin{aligned} \mathbf{w} &= w\hat{\mathbf{w}} = \mathbf{u} + \lambda'\hat{\mathbf{n}} = u\hat{\mathbf{u}} + \lambda'\hat{\mathbf{n}}, \\ w &= \sqrt{u^2 + (\lambda')^2}, \end{aligned} \tag{S18}$$

S174 the vector and rate of global coiling, respectively. Comparing again to [Uzunoğlu *et al.* \(2016\)](#)
S175 and [Güzelkardeşler & Şahiner \(2024\)](#), u is their ‘first alternative curvature’, and λ' their
S176 ‘second alternative curvature’. Generalized helices are obtained when the second alternative
S177 curvature vanishes, $\lambda' = 0$ ([Güzelkardeşler & Şahiner 2024](#)). Substituting the identity
S178 $\tan \lambda = \kappa/\tau$ into their expression for the second alternative curvature, $\frac{\kappa^2}{\kappa^2 + \tau^2} (\kappa/\tau)'$, clearly
S179 results in $\cos^2 \lambda \, d \tan \lambda / ds$, which reduces to simply $d\lambda / ds \equiv \lambda'$. Namely, the second
S180 alternative curvature is simply the rate of change in lead angle.

S181 For generalized helices ($\lambda = \text{const}$), $\mathbf{w} = \mathbf{u}$, $\hat{\mathbf{u}}' = \mathbf{w} \times \hat{\mathbf{u}} = -\lambda'(\hat{\mathbf{u}} \times \hat{\mathbf{n}}) = 0$, and there is a fixed
S182 coiling axis, coinciding with a fixed Darboux vector. However, in general, the vector \mathbf{w}
S183 defines a precession of the Darboux vector (recall that \mathbf{u} is the instantaneous rotation of the
S184 Frenet frame), and is itself not fixed. In some special cases, when $u = \text{const}$ and \mathbf{w} fixed, one
S185 can obtain the ‘modulated curves’ of [Nutbourne & Martin \(1988\)](#), better known as ‘curves of
S186 constant precession’ ([Scofield 1995](#)).

S187 A slant helix is, similarly, a class of precession curves that includes the generalized helix
S188 and the curves of constant precession as special cases. The defining feature of a slant helix is
S189 a constant angle between the principal normal of the curve, $\hat{\mathbf{n}}$, and some fixed direction in
S190 space. In generalized helices, that angle is 90° . [Izumiya & Takeuchi’s \(2004\)](#) necessary and
S191 sufficient condition for a slant helix translates, in the notation of this study, to the
S192 proportionality relationship $\lambda' = \sigma u$. In other words, second alternative curvature is
S193 proportional to first alternative curvature, with a proportionality constant σ . The global
S194 coiling vector becomes $\mathbf{w} = w\hat{\mathbf{w}} = u(\hat{\mathbf{u}} + \sigma\hat{\mathbf{n}})$, and $\hat{\mathbf{w}}$ defines a fixed axis of rotation (or coiling),
S195 though coiling rate, $w = u\sqrt{1 + \sigma^2}$, around the fixed axis generally varies. That can be
S196 verified by $\sqrt{1 + \sigma^2}\hat{\mathbf{w}}' = (\hat{\mathbf{u}} + \sigma\hat{\mathbf{n}})' = \mathbf{w} \times \hat{\mathbf{u}} + \sigma\mathbf{w} \times \hat{\mathbf{n}} = (\sigma u\hat{\mathbf{n}}) \times \hat{\mathbf{u}} + \sigma(u\hat{\mathbf{u}} \times \hat{\mathbf{n}}) = 0$.

S197 Finally, note that the lead angle, λ , is defined in the $\hat{\mathbf{t}}\hat{\mathbf{b}}$ plane, the *rectifying plane* of the
S198 space curve. For generalized helices, this plane contains the coiling axis, i.e. z -axis, and lead
S199 angle therefore is the angle between $\hat{\mathbf{t}}$ and the r - θ (or x - y) plane, perpendicular to the coiling
S200 axis; or the z -component of $\hat{\mathbf{t}}$ is $\sin \lambda$. That is no longer the case for slant helices. The
S201 rectifying plane now revolves around the coiling axis at a fixed tilt angle, given by $\arctan(\sigma)$.
S202 Lead angle is still defined in the rectifying plane, and therefore the tangent vector, $\hat{\mathbf{t}}$, which is
S203 also the unit velocity vector of the space curve w.r.t to arclength, is given in Cartesian
S204 coordinates by

$$\hat{\mathbf{t}} = (-\cos \lambda \sin \theta + c \sin \lambda \cos \theta) \hat{\mathbf{x}} + (\cos \lambda \cos \theta + c \sin \lambda \sin \theta) \hat{\mathbf{y}} + \sqrt{1 - c^2} \sin \lambda \hat{\mathbf{z}}, \quad (\text{S19})$$

where $c = \frac{\sigma}{\sqrt{1 + \sigma^2}} = \text{const}$,

S206 and $\lambda = \lambda(s)$, $\theta = \theta(s)$.

S207 S6 Logarithmic slant helix

S208 For the logarithmic slant helix, $u = \tilde{u}/s$. Consequently, $\lambda' = \sigma \tilde{u}'/s$ and $w = \tilde{w}/s$, where
S209 $\tilde{w} = \tilde{u} \sqrt{1 + \sigma^2}$. Given that $d\theta/ds = w$, it is straightforward to get relations comparable to
S210 conical helices for revolution angle and arclength, $\theta = \tilde{w} \ln(s/s_0)$ and $s = s_0 e^{\gamma \theta}$, where $\gamma = 1/\tilde{w}$
S211 (in this section, $\gamma \equiv \gamma_s$). Given $\lambda' = d\lambda/ds = \sigma u = c w = c d\theta/ds$ (c as in Eq.[S19]), lead angle
S212 increases linearly with revolution angle according to $\lambda = \lambda_0 + c\theta$. From these expressions one
S213 can obtain the position vector of the logarithmic slant helix, $x(\theta)\hat{\mathbf{x}} + y(\theta)\hat{\mathbf{y}} + z(\theta)\hat{\mathbf{z}}$, by
S214 integrating $(ds/d\theta)\hat{\mathbf{t}}(s)$ w.r.t to θ , given Eq.[S19] for $\hat{\mathbf{t}}(s)$,

$$z(\theta) = C_z + \sqrt{1 - c^2} s_0 e^{\gamma \theta} \left(\frac{\gamma^2 \sin(c\theta + \lambda_0) - c\gamma \cos(c\theta + \lambda_0)}{c^2 + \gamma^2} \right), \quad (\text{S20})$$

$$\begin{aligned} x(\theta) = C_x + \frac{\gamma s_0 e^{\gamma \theta}}{c^4 + 2c^2\gamma^2 - 2c^2 + \gamma^4 + 2\gamma^2 + 1} & (-c^4 \cos \lambda \cos \theta + c^3 \gamma \sin \lambda \cos \theta - 2c^3 \sin \lambda \sin \theta \\ & - c^2 \gamma^2 \cos \lambda \cos \theta - 3c^2 \gamma \sin \theta \cos \lambda + c\gamma^3 \sin \lambda \cos \theta + 3c\gamma \sin \lambda \cos \theta + 2c \sin \lambda \sin \theta \\ & - \gamma^3 \sin \theta \cos \lambda + \gamma^2 \cos \lambda \cos \theta - \gamma \sin \theta \cos \lambda + \cos \lambda \cos \theta), \end{aligned} \quad (\text{S21})$$

$$\begin{aligned} y(\theta) = C_y + \frac{\gamma s_0 e^{\gamma \theta}}{c^4 + 2c^2\gamma^2 - 2c^2 + \gamma^4 + 2\gamma^2 + 1} & (-c^4 \sin \theta \cos \lambda + c^3 \gamma \sin \lambda \sin \theta + 2c^3 \sin \lambda \cos \theta \\ & - c^2 \gamma^2 \sin \theta \cos \lambda + 3c^2 \gamma \cos \lambda \cos \theta + c\gamma^3 \sin \lambda \sin \theta + 3c\gamma \sin \lambda \sin \theta \\ & - 2c \sin \lambda \cos \theta + \gamma^3 \cos \lambda \cos \theta + \gamma^2 \sin \theta \cos \lambda + \gamma \cos \lambda \cos \theta + \sin \theta \cos \lambda), \end{aligned} \quad (\text{S22})$$

S216 where C_z, C_x, C_y are determined from initial conditions, and $\lambda = \lambda(\theta) = \lambda_0 + c\theta$. These
S217 expressions for $x(\theta), y(\theta)$ and $z(\theta)$, can be used in computer graphics to simulate shells that
S218 follow a logarithmic slant helix centerline.

S219 **S7 Web application**

S220 For this study, I have also written a WebGL application to help with creating images of shells,
S221 as in Fig. 1. Snapshot of the code, coinciding with the publication of this report, is available
S222 at <https://doi.org/10.5281/zenodo.19895626>.

S223 • WebApp options and parameters for Fig. 1A–C are Shell unchecked, Centerline spiral
S224 checked, Generating curve unchecked, and either Planispiral (panel A) or Circular
S225 helix (panel C) additionally selected. Pitch angle 69° , Roll angle 200° , $\lambda_0 = 0.22$,
S226 $\tilde{w} = 11.43$ ($\gamma = 0.0875$), $\sigma = 0$.

S227 • Parameters for Fig. 1E are Pitch angle 270, Roll angle 64, Shell and Multispirals
S228 checked, Generating curve unchecked. $\lambda_0 = 0.39$, $\tilde{w} = 9.38$ ($\gamma = 0.107$), $\sigma = 0$.

S229 • For Fig. 1F, Pitch angle 70, Roll angle 257. Shell, Centerline spiral, and Generating
S230 curve checked. $\lambda_0 = 0.22$, $\tilde{w} = 11.43$ ($\gamma = 0.0875$), $\sigma = 0$.

S231 • Parameters for Fig. 1G are Pitch angle 69, Roll angle 300, Shell deselected, Centerline
S232 spiral checked, Generating curve unchecked, $\lambda_0 = 0$, $\tilde{w} = 11.43$ ($\gamma = 0.0875$), $\sigma = 0.013$.

S233 • Parameters for Fig. 1H are Pitch angle 69, Roll angle 36, Shell deselected, Centerline
S234 spiral checked, Generating curve unchecked, $\lambda_0 = 0$, $\tilde{w} = 18.99$ ($\gamma = 0.0527$), $\sigma = 0.01$.

S235 • For Fig. 1I, Pitch angle 62, Roll angle 152, Shell, Centerline spiral, and Generating curve
S236 checked, $\lambda_0 = 0$, $\tilde{w} = 5.85$ ($\gamma = 0.171$), $\sigma = 0.21$.

S237 **S8 Supplementary references**

S238 Ackerly SC (1992). The structure of ontogenetic variation in the shell of *Pecten*.

S239 *Palaeontology* 35: 847–867.

- S240 Cameron RAD (1981). Functional aspects of shell geometry in some british land snails. *Biol J*
S241 *Linn Soc* 16: 157–167. <https://doi.org/10.1111/j.1095-8312.1981.tb01648.x>.
- S242 Chouaieb N, Goriely A, Maddocks JH (2006). Helices. *Proc Natl Acad Sci USA* 103: 9398–9403.
S243 <https://doi.org/10.1073/pnas.0508370103>.
- S244 Clarke RK, Grahame J, Mill PJ (1999). Variation and constraint in the shells of two sibling
S245 species of intertidal rough periwinkles (Gastropoda: *Littorina* spp.). *J Zool* 247: 145–154.
S246 [10.1111/j.1469-7998.1999.tb00978.x](https://doi.org/10.1111/j.1469-7998.1999.tb00978.x).
- S247 De Renzi M, Mayoral E (2024). Understanding behaviour through theoretical morphology:
S248 the case of helical-shaped burrows. *J Iber Geol* 50: 549–566.
S249 <https://doi.org/10.1007/s41513-024-00249-7>.
- S250 Ekaratne SUK, Crisp DJ (1983). A geometric analysis of growth in gastropod shells, with
S251 particular reference to turbinate forms. *Journal of Marine Biology Association UK* 63:
S252 777–797.
- S253 Goriely A (2017). *The Mathematics and Mechanics of Biological Growth*. Springer.
S254 <https://doi.org/10.1007/978-0-387-87710-5>.
- S255 Güzelkardeşler G, Şahiner B (2024). An alternative approach to find the position vector of a
S256 general helix. *Celal Bayar University Journal of Science* 20: 54–60.
S257 [10.18466/cbayarfbe.1479066](https://doi.org/10.18466/cbayarfbe.1479066).
- S258 Hauser K, He Y, Garcia-Diaz M, Simmerling C, Coutsiar E (2017). Characterization of
S259 biomolecular helices and their complementarity using geometric analysis. *Journal of*
S260 *Chemical Information and Modeling* 57: 864–874.
S261 <https://doi.org/10.1021/acs.jcim.6b00721>. PMID: 28287728.
- S262 Illert C (1983). The mathematics of gnomonic seashells. *Math Biosci* 63: 21–56.
- S263 Izumiya S, Takeuchi N (2004). New special curves and developable surfaces. *Turkish Journal*
S264 *of Mathematics* 28: 153–164.
- S265 Kemp P, Bertness MD (1984). Snail shape and growth rates: evidence for plastic shell
S266 allometry in *Littorina littorea*. *Proc Natl Acad Sci USA* 81: 811–813.

S267 <https://doi.org/10.1073/pnas.81.3.811>.

S268 Kohn AJ, Riggs AC (1975). Morphometry of the *Conus* shell. *Syst Zool* 24: 346–359.

S269 Larsson J, Westram AM, Bengmark S, Lundh T, Butlin RK, Butlin RK (2020). A
S270 developmentally descriptive method for quantifying shape in gastropod shells. *J R Soc*
S271 *Interface* 17. <http://dx.doi.org/10.1098/rsif.2019.0721>.

S272 Løvtrup S, von Sydow B (1974). D’arcy Thompson’s theorem and the shape of the molluscan
S273 shell. *Bull Math Biol* 36: 567–575.

S274 McGhee GR (1999). *Theoretical Morphology : The Concept and Its Applications*. Perspectives in
S275 Earth History and Paleobiology. Columbia University Press, New York.

S276 McNair C, Kier W, LaCroix P, Linsley R (1981). The functional significance of aperture form
S277 in gastropods. *Lethaia* 14: 63–70.

S278 Moseley H (1842). On conchylometry. *Lond Edinb Dubl Phil Mag* 21: 300–305.

S279 Moulton D, Goriely A, Chirat R (2012). Mechanical growth and morphogenesis of seashells. *J*
S280 *Theor Biol* 311: 69–79. <https://doi.org/10.1016/j.jtbi.2012.07.009>.

S281 Moulton DE, Goriely A (2012). Surface growth kinematics via local curve evolution. *J of*
S282 *Math Biol* 68: 81–108.

S283 Newkirk GF, Doyle RW (1975). Genetic analysis of shell-shape variation in *Littorina saxatilis*
S284 on an environmental cline. *Mar Biol* 30: 227–237. [10.1007/BF00390745](https://doi.org/10.1007/BF00390745).

S285 Noshita K, Asami T, Ubukata T (2012). Functional constraints on coiling geometry and
S286 aperture inclination in gastropods. *Paleobiology* 38: 322–334. [10.1666/10060.1](https://doi.org/10.1666/10060.1).

S287 Nutbourne AW, Martin RR (1988). *Differential geometry applied to curve and surface design:*
S288 *Foundations*. Ellis Horwood, Chichester, England.

S289 O’Neill B (2006). *Elementary Differential Geometry*. Revised 2nd edn. Academic Press.

S290 Raup DM (1961). The geometry of coiling in gastropods. *Proc Natl Acad Sci USA* 47: 602–609.
S291 <https://doi.org/10.1073/pnas.47.4.602>.

S292 Raup DM (1966). Geometric analysis of shell coiling: general problems. *J Paleontol* 40:
S293 1178–1190.

S294 Raup DM, Graus RR (1972). General equations for volume and surface area of a
S295 logarithmically coiled shell. *Mathematical Geology* 4: 307–316.

S296 Raup DM, Michelson A (1965). Theoretical morphology of the coiled shell. *Science* 147:
S297 1294–1295.

S298 Schindel DE (1990). Unoccupied morphospace and the coiled geometry of gastropods:
S299 architectural constraint or geometric covariation? In *Causes of Evolution: a paleontological*
S300 *perspective* (edited by Ross R, Allmon W), pp. 270–304. University of Chicago Press,
S301 Chicago.

S302 Scofield PD (1995). Curves of constant precession. *The American Mathematical Monthly* 102:
S303 531–537. <https://doi.org/10.1080/00029890.1995.12004613>.

S304 Stone JR (1995). CerioShell: a computer program designed to simulate variation in shell form.
S305 *Paleobiology* 21: 509–519.

S306 Thompson DW ([1942] 1992). *On Growth and Form: The Complete Revised Edition*. Dover,
S307 New York.

S308 Urdy S, Goudemand N, Bucher H, Chirat R (2010). Allometries and the morphogenesis of the
S309 molluscan shell: a quantitative and theoretical model. *J Exp Zool* 314B: 280–302.
S310 [10.1002/jez.b.21337](https://doi.org/10.1002/jez.b.21337).

S311 Uzunoğlu B, İsmail Gök, Yaylı Y (2016). A new approach on curves of constant precession.
S312 *Applied Mathematics and Computation* 275: 317–323.
S313 <https://doi.org/10.1016/j.amc.2015.11.083>.

S314 Vermeij GJ (1993). *A Natural History of Shells*. Princeton University Press, Princeton, Oxford.